Study of Sample Dispersion Mechanisms in an Electroosmotically Pumped Microchannel

B. Debusschere*, H. Najm*, A. Matta†, O. Knio†, R. Ghanem†, and O. Le Maître‡

* Sandia National Labs, Livermore, CA, bjdebus@ca.sandia.gov
† The Johns Hopkins University, Baltimore, MD
‡ Université d'Evry Val d'Essonne, Evry, France

ABSTRACT

This paper presents detailed simulations of electroosmotic microchannel flow to study the effect of species charge, chemical reaction and random ζ potential variability on both elektrokinetic and hydrodynamic dispersion. The physical model used accounts for the coupled nature of momentum, species transport and reactions, as well as the electrostatic field. The chemistry model accounts for pH-dependent protein labeling reactions as well as detailed buffer electrochemistry. Using polynomical chaos expansions, the model also accounts for stochastic ζ potential variability due to heterogeneous wall surface properties. The results show that dispersion increases for higher species charges and for larger variability in ζ. The dispersion also depends mildly on the correlation length of the ζ potential variability.

Keywords: Sample Dispersion, Simulation, Microchannel, Polynomial Chaos, Labeling

1 INTRODUCTION

In many microfluidic separation processes, dispersion of sample peaks is a significant problem limiting the spatial detection resolution. Common causes of dispersion in electrophoretic separations include electrokinetic and hydrodynamic dispersion, wall adsorption of the analyte, and mobility variations associated with transverse temperature gradients [1]. Electrokinetic dispersion is caused by non-uniformities in the conductivity and pH of the fluid, triggered by the movement of charged analytes. Hydrodynamic dispersion is caused by a non-uniform bulk velocity profile, typically associated with pressure gradients in the channel. To maximize the separation resolution, these dispersion sources need to be minimized by careful selection of sample and buffer parameters, as well as control of the microchannel fabrication process.

In this work, we use detailed simulations to study electrokinetic and hydrodynamic dispersion during protein transport and labeling processes in electroosmotic microchannel flow. We specifically address two phenomena. The first is the electrokinetic and hydrodynamic dispersion, caused by the disturbance of the buffer solution as a sample of charged analyte moves through the channel. The second is the effect on sample dispersion of a random ζ-potential variability, due to heterogeneous surface roughness or wall material properties.

Next, we will outline the formulation of the model used in the computations. The following section then shows the results of applying this model to the cases described above.

2 FORMULATION

Microchannel flows, involving electroosmotic flow of charged components in an electrolyte buffer, are generally characterized by strong coupling between multiple physical and chemical processes [2]. A detailed study of analyte dispersion therefore requires accurate models for the fluid flow, species transport, chemical reactions, buffer equilibrium, electrostatic field strength, wall layer, and many other processes. To this end, the simulation code developed in this work [3, 4] solves the coupled momentum, species conservation, as well as electrostatic field equations. An empirical ζ potential model takes into account variations in buffer pH and molarity. The chemistry model accounts for pH-dependent protein labeling reactions as well as detailed buffer electrochemistry in a mixed finite-rate/equilibrium formulation.

The model also has the unique capability to account for the effect of stochastic processes, such as a ζ-potential with random variability, given by the expression

$$\zeta = \zeta_0(\mathrm{pH}, \mathcal{M}) \times (1 + g(x, \theta)) \qquad (1)$$

In this equation, ζ_0 represents the nominal ζ potential, and $g(x, \theta)$ the random variability of this ζ potential due to heterogeneous wall surface properties. The dependence of g on the variable θ denotes the stochastic character of this variability, which is assumed to be a Gaussian process with an auto-correlation function C, given by

$$C(|x_1 - x_2|) = \sigma_g^2 \exp(-|x_1 - x_2|/L_c) \qquad (2)$$

L_c is the correlation length and σ_g the standard deviation of g. Using a Karhunen-Loève expansion in terms of the eigenfunctions of the auto-correlation function C,

the stochastic ζ potential can be expressed as a Polynomial Chaos (PC) expansion [5–7]:

$$\zeta(x,t,\theta) = \sum_{k=0}^{P} a_k(x,t)\Psi_k(\theta) \tag{3}$$

with mode strengths a_k and Hermite polynomials Ψ_k. All flow variables are similarly represented with PC expansions. After substituting these expansions into the governing equations, a Galerkin procedure is used to obtain evolution equations for the spectral mode strengths of the dependent variables [3, 4, 7]. The zero-th order mode of each quantity represents the mean of this quantity over all realizations. The variation around this mean is given by the higher order modes.

To quantify dispersion, the square of the width of a concentration profile c was calculated at each point in time as

$$\delta^2 = \overline{x_c^2} - \overline{x_c}^2 \tag{4}$$

with $\overline{x_c}$ and $\overline{x_c^2}$ defined as

$$\overline{x_c}(t,\theta) = \frac{\int_0^{L_x} x\ c(x,t,\theta)\ dx}{\int_0^{L_x} c(x,t,\theta)\ dx} \tag{5}$$

$$\overline{x_c^2}(t,\theta) = \frac{\int_0^{L_x} x^2\ c(x,t,\theta)\ dx}{\int_0^{L_x} c(x,t,\theta)\ dx} \tag{6}$$

For concentrations with a Gaussian profile, the width δ varies in time as

$$\delta^2(t_2) = \delta^2(t_1) + 2D_{\text{eff}}(t_2 - t_1) \tag{7}$$

where D_{eff} is the effective diffusion coefficient, representing the combined effect of molecular diffusion and dispersion [8]. Note that while the flow field is still developing, δ^2 typically does not grow linearly in time. However, for the late time behavior, equation (7) generally holds.

3 RESULTS

The model described above was used to study the dispersion of analyte plugs in two-dimensional microchannel flows, with a geometry as in figure 1. In all simulations, the flow was initialized with a 1 mM uniform potassium phosphate buffer at a pH of 7.25. A model protein U and a dye D were introduced with an initially Gaussian profile. Two types of cases were studied: reacting flows with deterministic ζ potential, and non-reacting flows with stochastic ζ potential variability.

In the first set of simulations, U was each time given a different (but fixed) positive charge, and D the opposite charge. Both had an initial concentration of 10^{-5} mol/l. Due to the combined effect of the bulk electroosmotic convection and electrophoresis, the U plug crosses the D plug, allowing the formation of a neutral labeled protein

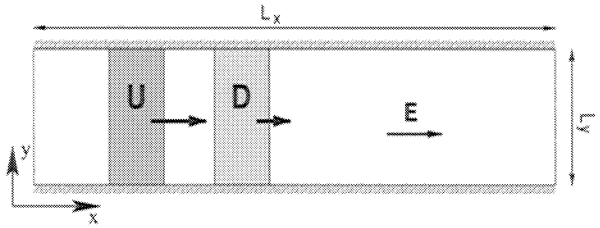

Figure 1: Simulation geometry: a plug of protein U and dye D are introduced in a rectangular microchannel with an electroosmotic bulk flow.

L according to the model irreversible protein labeling reaction

$$\mathrm{U} + \mathrm{D} \xrightarrow{k_L} \mathrm{L} \tag{8}$$

Figure 2 shows a typical snapshot of both the L profile and the streamwise convection velocity u, shortly after the U and D plugs have crossed and reacted. In this specific case, U had a charge of +6 and D a charge of -6, in a channel that was 1 cm long and 100 μm deep. The distortion in this L profile is caused by the transport

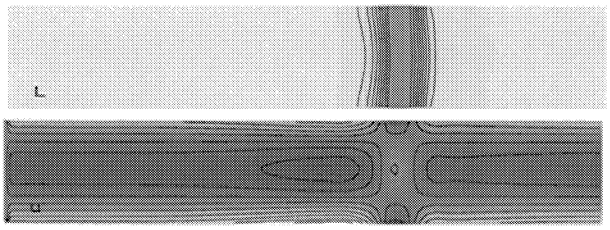

Figure 2: Contour plot of the labeled protein concentration (top) and the streamwise convective velocity (bottom) after reaction of a band of U^{6+} and D^{6-} in a 100 μm deep channel. Darker background color means larger values. The full domain is shown but the wall-normal dimension is stretched for clarity.

and reaction of the U and D ions, which disturb the electrolyte buffer as well as the electrical conductivity. The conductivity changes consequently cause disturbances in both the streamwise and wall-normal electrostatic field strength. Besides the electrokinetic dispersion caused by these non-uniformities in the electrostatic field, the variations in the streamwise field strength also cause local changes in the electroosmotic wall velocities. This induces pressure gradients and a corresponding hydrodynamic dispersion from non-uniform convection velocity profiles. In figure 2, a locally higher electrostatic field strength increases the electroosmotic wall velocity near the L plug, which causes pressure gradients before and after the L plug.

For dispersion quantification, three cases were run, corresponding to a charge on U of +1, +2, and +4 (and a charge on D of -1, -2 , and -4 respectively). Each

time, the domain was 4 cm long and 100 μm deep. The initial U and D plugs were located at $x = 0.2$ cm and $x = 0.4$ cm respectively. The resulting dispersion of the different profiles, along with their effective diffusion coefficients, obtained from equation (7), are summarized in figure 3. Note that for charges more negative than

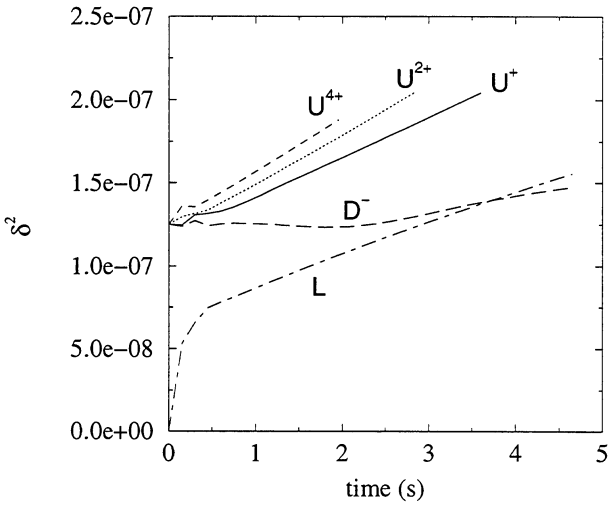

Figure 3: Time evolution of profile widths for the reacting cases with specified charges for U and D, but without random ζ potential variability. The dispersion for U increases as its charge increases. Effective diffusion coefficient (in 10^{-8} m^2/s) for the curve labeled U$^+$: 1.21; U^{2+}: 1.51; U^{4+}: 1.63; D$^-$: 0.51; L: 0.94.

-1, electrophoresis moves the D plug faster upstream than the electroosmotic flow velocity. Since this moves D out of the domain on the left side early on, no data on D for these cases is shown. Except for very early times, the behavior of the L width was identical in all three runs, and therefore only the data of one case is shown (corresponding to U$^+$). Overall, the dispersion of the positively charged protein increases with increasing charge. The dispersion of D$^-$ is much smaller, and the width of D$^-$ even decreases early on. This decrease is caused by disturbances in the electrical conductivity, left in the wake of the U$^+$ plug, that tend to sharpen the D$^-$ profile.

In a second set of simulations both U and D were held neutral and non-reacting. A random ζ potential variability was imposed on the top wall, with various choices for the coefficients of variation (COV) and the correlation lengths L_c. Each time, four modes were used in the Karhunen-Loève expansion of the ζ potential variability. The channel size was 1 cm long by 100 μm deep. The ζ potential variations in these cases cause disturbances in the convective velocity profile, leading to hydrodynamic dispersion.

Figure 4 shows the time evolution of the mean squared

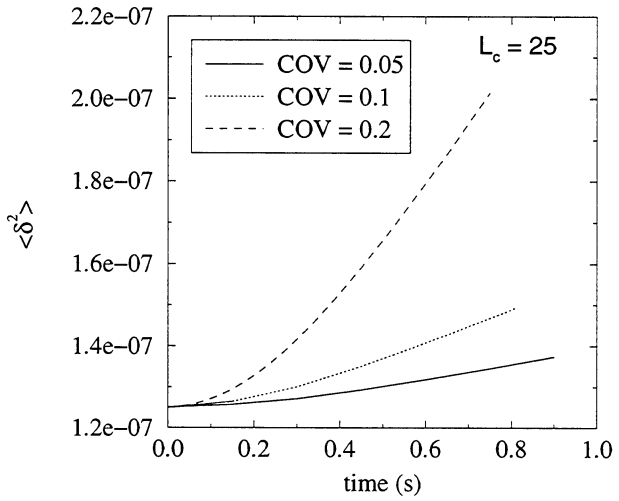

Figure 4: Time evolution of the mean profile widths for the non-reacting cases having a random ζ potential variability with $L_c = 25$ channel depths. The dispersion increases as the COV of the ζ variability increases. Effective diffusion coefficient (in 10^{-8} m^2/s) for COV = 0.05: 0.91; COV = 0.1: 1.99; COV = 0.2: 7.00

profile widths of U, for a COV ranging from 0.05 to 0.2. The ζ potential variability correlation length for these cases was 25 channel depths. Note that this mean $< \delta^2 >$ corresponds to the mean of the widths of the profiles corresponding to all possible realizations of ζ potential profiles that have the given statistical variability. As the COV increases, figure 4 clearly shows a strong increase in the predicted dispersion. Figure 5 shows the results for the same runs, but with a correlation length $L_c = 50$ channel depths, so the ζ potential varies on a longer length scale. The dispersion in these cases is slightly higher than for the corresponding cases with the shorter correlation length.

Beyond the mean behavior of the profile width, the stochastic methodology also gives full statistical information about this quantity. Figure 6 for example shows the pdf of δ^2 at $t = 0.75$ s, representing the range of widths for U at this point in time, corresponding to all possible ζ potential profile realizations. The probability density function in figure 6 indicates the upper and lower dispersion bounds for the U profile. This knowledge allows for reliability assessments of electrophoretic separation devices that have non-uniform wall surface properties due to for example the microchannel fabrication process or impurities in the wall material.

4 CONCLUSIONS

In this work, simulations were performed of electroosmotic microchannel flow to study electrokinetic and hydrodynamic dispersion of sample peaks during protein transport and labeling processes. The physical model

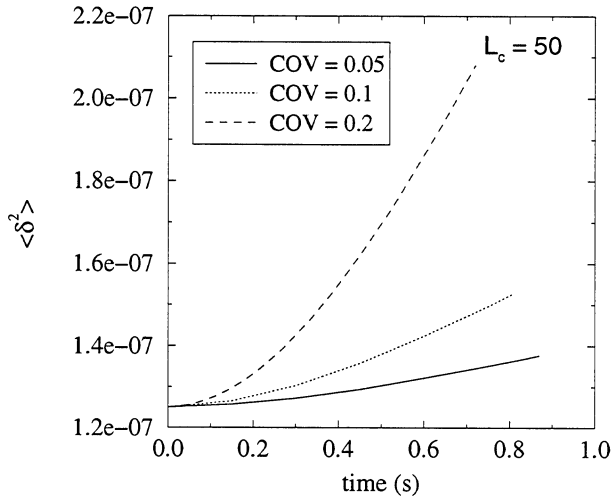

Figure 5: Time evolution of the mean profile widths for the non-reacting cases having a random ζ potential variability with $L_c = 50$ channel depths. The dispersion is slightly larger than for the shorter correlation length case. Effective diffusion coefficient (in 10^{-8} m^2/s) for COV = 0.05: 0.98; COV = 0.1: 2.38; COV = 0.2: 8.55

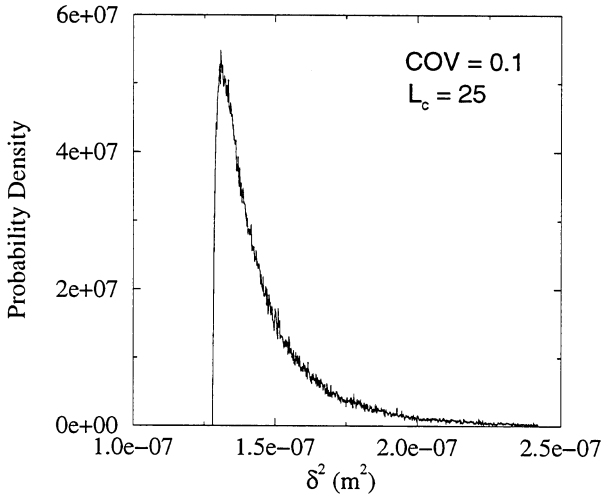

Figure 6: Probability density function for the width (squared) of the U profile at $t = 0.75$ s in a case with $L_c = 25$, COV = 0.1. This pdf represents the variability in the dispersion over all realizations of ζ.

used incorporates the coupled nature of momentum transport, species transport and reaction, the electrostatic field, as well as a full representation of the electrolyte buffer reactions and the dependence of the ζ potential on the local buffer properties. Furthermore, a stochastic methodology was used to account for the effect of random ζ potential variability, using polynomial chaos expansions for the stochastic ζ potential and field variables.

For the cases with a labeling reaction between a positively charged protein and a negatively charged dye, the dispersion was found to increase for higher species charges. In the cases with stochastic ζ potential variability, the dispersion increased with higher coefficients of variation for ζ. The dispersion also appears to depend mildly on the correlation length of the ζ potential variability.

Overall, the microchannel simulation code developed in this work is a powerful tool to study dominant sample dispersion mechanisms. Because it can predict peak dispersion including upper and lower bounds, it also allows for reliability assessments in the design of electrophoretic separation devices.

ACKNOWLEDGMENT

This work was supported by the Defense Advanced Research Projects Agency (DARPA) and Air Force Research Laboratory, Air Force Materiel Command, USAF, under agreement number F30602-00-2-0612. The U.S. government is authorized to reproduce and distribute reprints for governmental purposes notwithstanding any copyright annotation thereon.

REFERENCES

[1] Roberts, G.O., Rhodes, P.H., and Snyder, R.S., *J. Chromatogr.*, 480:35–67 (1989).

[2] Thormann, W., and Mosher, R.A., *Adv. Electrophoresis*, 2:45–108 (1988).

[3] Debusschere, B., Najm, H., Matta, A., Shu, T., Knio, O., Ghanem, R., and Le Maître, O., *Proc. 5th Int. Conf. on Modeling and Simulation of Microsystems*, pp. 384–387, (2002).

[4] Debusschere, B.J., Najm, H.N., Matta, A., Knio, O.M., Ghanem, R.G., and Le Maître, O.P., *Phys. Fluids* (2002) submitted.

[5] Ghanem, R.G., and Spanos, P.D., *Stochastic Finite Elements: A Spectral Approach*, Springer Verlag, (1991).

[6] Wiener, N., *Amer. J. Math.*, 60:897–936 (1938).

[7] Le Maître, O.P., Reagan, M.T., Najm, H.N., Ghanem, R.G., and Knio, O.M., *J. Comp. Phys.*, 181:9–44 (2002).

[8] Ghosal, S., *Analytical Chemistry*, 74(16):4198–4203 (2002).